Proceedings of the 10th World Congress on Mechanical, Chemical, and Material Engineering (MCM'24)
Barcelona, Spain –August 22-24, 2024
Paper No. HTFF 208
DOI: 10.11159/htff24.208

Optimization of a Novel Air-Curtain-Sealed Personal Protective Equipment – A CFD Approach

Nuno Rosa, Joel Loureiro, José Costa, Adélio Gaspar, Manuel Gameiro
Univ Coimbra, ADAI, Department of Mechanical Engineering
Rua Luís Reis Santos, Pólo II, 3030-788 Coimbra, Portugal
nuno.rosa@uc.pt; j9loureiro@gmail.com; jose.costa@dem.uc.pt; adelio.gaspar@dem.uc.pt; manuel.gameiro@dem.uc.pt

Abstract **–** This paper presents the optimization of a novel air-sealed visor for medical care using computational fluid dynamics (CFD). The personal protective equipment (PPE) provides aerodynamic sealing of the breathing zone, thereby reducing the risk of inhaling droplets and aerosols carrying viruses. To ensure a uniform and stable air-curtain, the air supply system was designed to maintain uniform jet velocities of 0.5 m/s at the forefront jet slots and 1.0 m/s at the lateral jet slots. The main parameters under study are the air curtain stability and the volume of contaminated air in the breathing zone. The impact of tilt angle, velocity of the jets, and human breathing was assessed. Three turbulence models - RNG k-ε, SST, and BSL - were tested to assess their suitability for airflow field modeling.

Keywords**:** PPE, CFD, Aerodynamic sealing, Air-sealed visor, Infection barrier

1. Introduction

The COVID-19 pandemic raised concerns regarding the safety of frontline healthcare workers, particularly those in close contact with patients for prolonged periods [1]. Among these, dentists were identified as being at particularly high risk due to the nature of their work, which involves proximity to the patient's mouth and the generation of aerosols during dental procedures [2], [3]. Efforts to mitigate the risk of transmission among dental professionals have centered around the use of personal protective equipment (PPE), including masks, face shields, gloves, and gowns [4]–[6]. Respirators, such as N95 masks, have been recommended due to their effectiveness in reducing exposure to aerosols [7]. However, the extended use of respirators has been associated with discomfort and physiological challenges [8], [9]. While face shields have been touted as an effective addition to face masks for blocking droplets [10], they have shown low efficacy in preventing aerosol transmission [11]. In response to these challenges, researchers have explored alternative approaches, such as the use of air-curtain devices, to provide additional protection against airborne contaminants [12]–[15]. These devices create a barrier of moving air in front of the face which can block and redirect contaminants away from the wearer, thereby improving air quality and reducing the risk of exposure. This paper focuses on the optimization of a novel air-sealed visor [16]–[18]. The PPE consists of a front shield, an air-supply plenum, and a complex support system. It aims to provide aerodynamic sealing of the breathing zone, thereby reducing the risk of inhaling droplets and aerosols carrying a potential viral load. To assess its efficacy, a combination of numerical simulations was conducted, focusing on factors such as jet air velocity, title angle, and breathing dynamics. Additionally, this study offers insights into the selection of appropriate turbulence models for simulating similar airflow scenarios, comparing the performance of the RNG k-ε, Shear Stress Transport (SST), and BSL Reynolds stress models. The protection effect, assessed as a sealing efficiency, provided by the original device (with jet velocities of 0.5 m/s at the forefront jet slots and 1.0 m/s at the lateral jets slots) was approximately 68.3 %, based on the numerical results with the RNG turbulence model.

2. CFD Model

2.1. The air-curtain personal protective equipment

The air-curtain PPE is designed to be comfortable and compatible with face masks, respirators, and dental equipment. Fig. 1 illustrates the prototype, consisting of a face shield (A), air-curtain plenum (B), and support system (D and E). The face shield protects against larger droplets from dental equipment. Air is supplied by a dental air compressor through an 8 mm diameter tube (C in Fig. 1a), splitting into two inlets before reaching the plenum. The plenum features eight outlets, ensuring a uniform air velocity across slots 1, 2, and 3 (≈0.5 m/s) and higher velocity (≈1.0 m/s) in outlet L (Fig. 1b). The

inner plenum geometry maintains uniform pressure drop at all outlets. Flow control is achieved through polymeric perforated barriers (I in Fig. 1b) and a wall upstream of the jet slots (M in Fig. 1b). Two polymeric covers are assembled using four screws (J in Fig. 1b), while a cog wheel-buckle system in the support enables adjustment for users of different head sizes. For further details and initial design models, refer to previously published work [16]–[18].

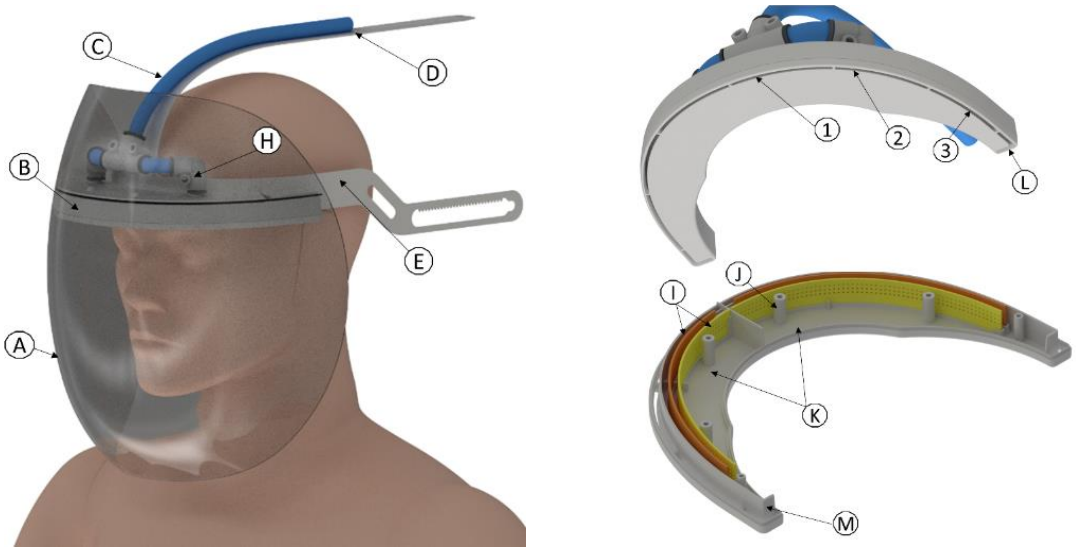

a) Face Shield components. b) Plenum geometry.

Fig. 1: Air-curtain-sealed personal protective equipment [17].

2.2. CFD Setup

The CFD simulations were conducted using ANSYS CFX®. A multicomponent flow model was used, employing two fluids with identical properties: "clean air" blown through the plenum slots, establishing wall jets inside the visor for sealing and safety, and "contaminated air" surrounding the user. This model simulates the flow and mixing between the two fluids, verifying PPE protection in extreme contamination scenarios. The PPE protective factor can be calculated using Equation [19]:

$$PF\ (\%) = \left(1 - \frac{N_i}{N_o}\right) \times 100 \tag{1}$$

considering N_i as the contaminated air in the breathing zone, inside the PPE, and N_o as the contaminated air in front and outside of the PPE. The SST, RNG k-ε, and BSL models were used to predict turbulence effects and fluid mixing. Transient simulations with a 0.1 s time step and a total time of 10s ensured convergence. Initial conditions assumed clean air within the visor safety domain and contaminated air around the user. Boundary conditions included a contaminated air opening-type boundary with 0 Pa pressure and 5% turbulence intensity, and a clean air inlet with jet air velocity profiles. In the plenum model, conditions involved an inlet mass flow rate of 24.5 l/min and 0 Pa pressure in the outlets. Breathing air flow rate was modelled using a harmonic function based on Giu and Niu work [20]:

$$\dot{Q} = 0.14 \sin(1.8t) \tag{2}$$

The breathing process was only considered through the nose, considering an area ($A_n \approx 149\times 10^{-6}$ m^2) taken from the 3D scanned CAD model. A matrix of 12 points at the nose level and 26 points at the mouth level were used to

calculate the volume fraction of contaminated air. An unstructured tetrahedral grid was setup for the spatial domains' discretization. The grid was refined in important areas such as air supply, manikin head, and visor walls, to reach a non-dimensional near-wall distance $y^+ < 1$ in the airflow domain. Grid dependence tests were carried out to ensure that the numerical results were grid-independent leading to a total of ≈ 1.7 million nodes and ≈ 6.3 million cells.

Three studies were conducted: the optimization of the original prototype presented in reference [16] without considering the breathing effect, then analyzing of the impact of breathing on the original prototype and finally studying of the influence of breathing on the optimized version. The jet velocities and the tilt angle of the lateral jet (L in Fig.1) were analyzed to maximize the PF. Different sets of jet velocity values were studied, where V_1, V_2, V_3, and V_L (Table 1) represent the magnitude of the outlet velocity for jets 1, 2, 3, and L, respectively. V_L was calculated to ensure that the momentum of the lateral jet equaled the combined momentum of the other three jets, aiming to mitigate or reduce the entrainment of air from this jet into the breathing zone. For the given set of jet velocities, the tilt angle of the fourth jet, Θ_4, was adjusted in increments of 20°, ranging from 0° to 80°.

3. Results and Discussion

3.1. Jets air velocity

The PF results for various velocity sets are outlined in Table 1. Upon analysis, it is evident that the concept behind the chosen jet velocity sets generally yielded higher PFs.

Table 1: Sets of jet velocity values considered for the optimization study and PF results.

Velocity set	V_1	V_2	V_3	V_L	PF		
	[m /s]				RNG Model	SST Model	BSL Model
S1	0.5	0.5	0.5	1.74	27.0 %	59.3 %	61.3 %
S2	0.4	0.4	0.4	1.39	48.0 %	77.4 %	74.0 %
S3	0.3	0.3	0.3	1.04	56.0 %	83.6 %	82.9 %
S4	0.2	0.2	0.2	0.70	92.4 %	79.3 %	79.3 %
S5	0.1	0.1	0.1	0.35	100.0 %	100.0 %	100.0 %
S6	0.6	0.6	0.4	1.91	2.7 %	75.6 %	66.2 %

As jet velocities decrease, higher levels of protection are achieved. This occurs because lower jet velocities lead to reduced momentum of the air curtain, particularly in the frontal jets. Consequently, there is an earlier separation of the airflow from the visor shield, illustrated in Fig. 2, which boosts air circulation around the user's face and dilutes contaminated air. A stable air curtain that adheres to the visor shield for a longer distance, in these conditions, does not correspond to higher values of PF. Conversely, the air circulation near the user's face might have negative effects, such as dryness of the mucous membranes.

A significant difference was observed between the values of the RNG model and the other two models, which showed similar outcomes. The RNG model results shown a considerably more stable air curtain compared to the other models, as illustrated in Fig. 2. Consequently, it did not promote a strong mixture between contaminated air and clean air, thereby facilitating the entry of contaminated air. The last velocity set exemplified this behavior effectively. Taking the aforementioned factors into account, the first and fourth velocity sets were selected for further analysis. The first set was preferred due to its favorable air curtain characteristics for user comfort, while the fourth set was chosen for its optimal contaminant distribution in the mid-plane, as illustrated in Fig. 3 for the RNG model.

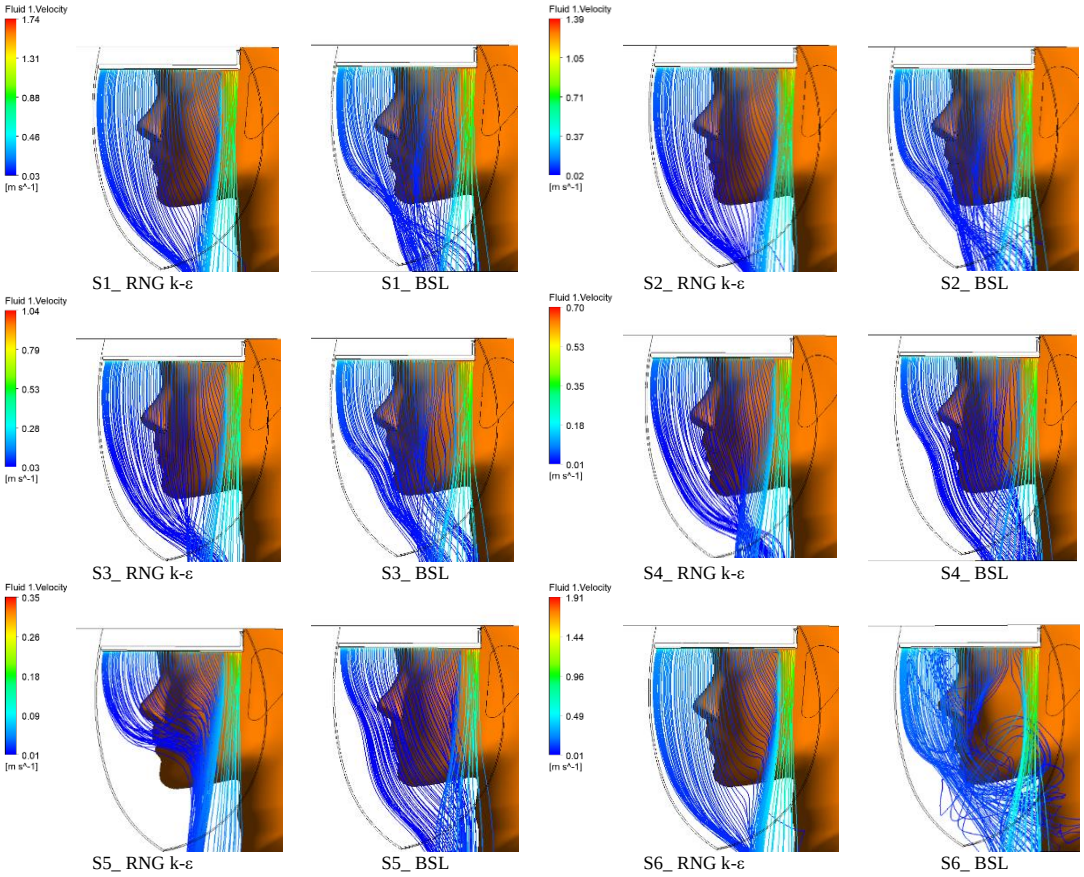

Fig. 2: Streamlines of the airflow inside the PPE for the different velocity sets.

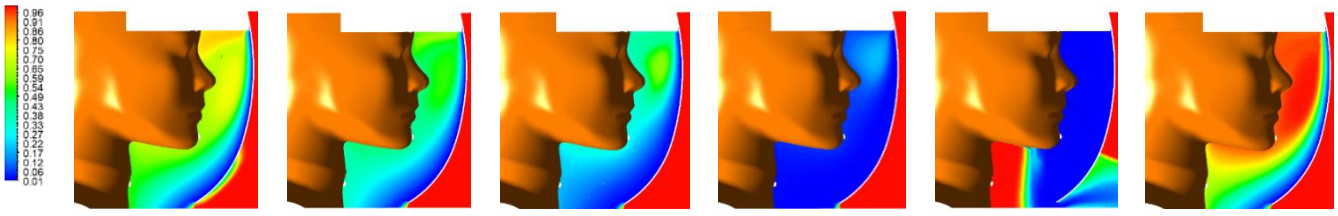

Fig. 3: Volume fraction of contaminated air in the mid-plane for each velocity set (e.g. RNG model).

3.2. Tilt angle of the lateral jet

The PFs results for the different tilt angles are displayed in Fig. 4a) and b) for the first and fourth velocity sets, respectively. Analyzing Fig. 4a) one could conclude that, for the first velocity set, the optimal tilt angle of the lateral jet was 20°. This angle allowed the sealing of the space between the user's face and the visor, through which contaminated air could easily enter, as can be seen in Fig. 5a) and b). For higher values of this angle, the air coming out of the lateral jet started to get entrained into the visor's interior, which led to lower PFs. An exception was observed for the RNG model at a tilt angle of 60°. At $\theta_4 = 0°$, the sealing of the breathing zone was inadequate, despite minimal suction of the lateral jet's air. Upon examining Fig. 4b), it became evident that for the fourth velocity set, the optimal tilt angle of the fourth jet was 0°. Higher angles resulted in increased entrainment of the lateral jet's air, leading to lower PFs. It is also important to note that, for this velocity set, the air curtain presented fewer vortices, especially in the breathing zone,

contributing to lower PFs compared to the first velocity set (Fig. 5b). Once again, the results for the RNG model differed significantly from those obtained for the SST and BSL models.

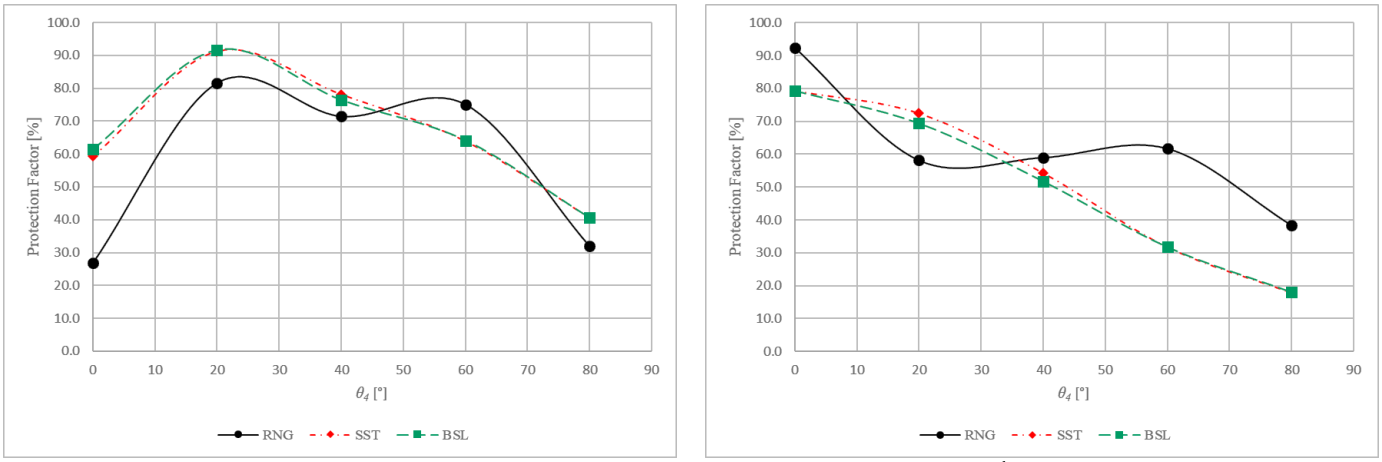

a) 1st velocity set b) 4th velocity set

Fig. 4: Protection factor variation with the tilt angle of the 4th jet.

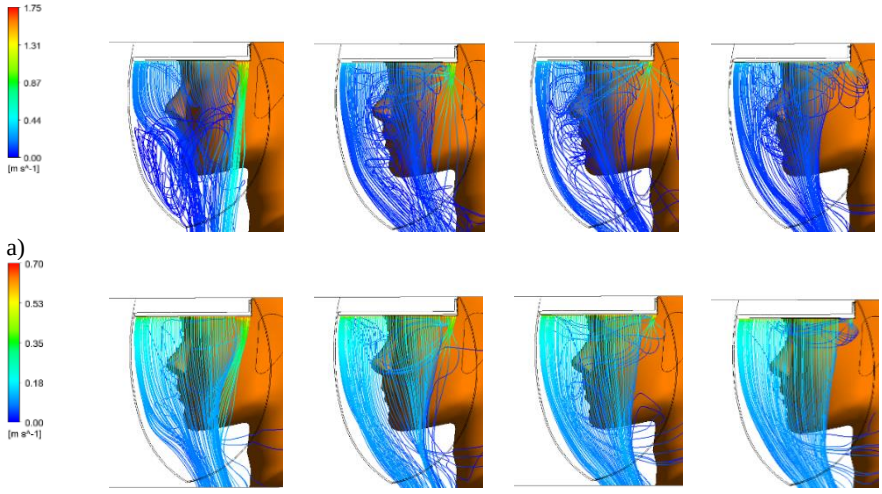

Fig. 5: Streamlines of the airflow for each value of θ_4 for the SST model with the 1st (a) and 4th (b) velocity sets.

3.3. Breathing effect

The PFs with and without the breathing effect, obtained for the original prototype [16] and each turbulence model, are presented in Table 2.

Table 2: PFs of the original prototype with breathing and without breathing.

	RNG Model	SST Model	BSL Model
PF with breathing	44.6 %	49.6 %	49.7 %
PF without breathing	68.2 %	45.5 %	45.5 %

The RNG model is once again shown to have a different behavior from the other two models, as can be seen in Fig. 6a) and b) for the contaminant fraction evolution, and in Fig. 7a) and b) for the streamline's evolution, respectively. Analyzing

the PFs and contaminant fraction evolutions, the RNG model showed a drop in performance, while the other two models showed improvement. Breathing significantly affects the air curtain: expiration breaks the curtain, promoting cleaning respiratory zone, while inspiration leads to air aspiration from the lateral and third jets, reducing sealing efficiency. The and BSL models predict more vortices and a less stable air curtain, facilitating the mixing of contaminated and cleaned and resulting in better performance during respiration. Notably, the PF significantly drops for the RNG model with due to its more stable air curtain without respiration, leading to less entrainment from the fourth jet.

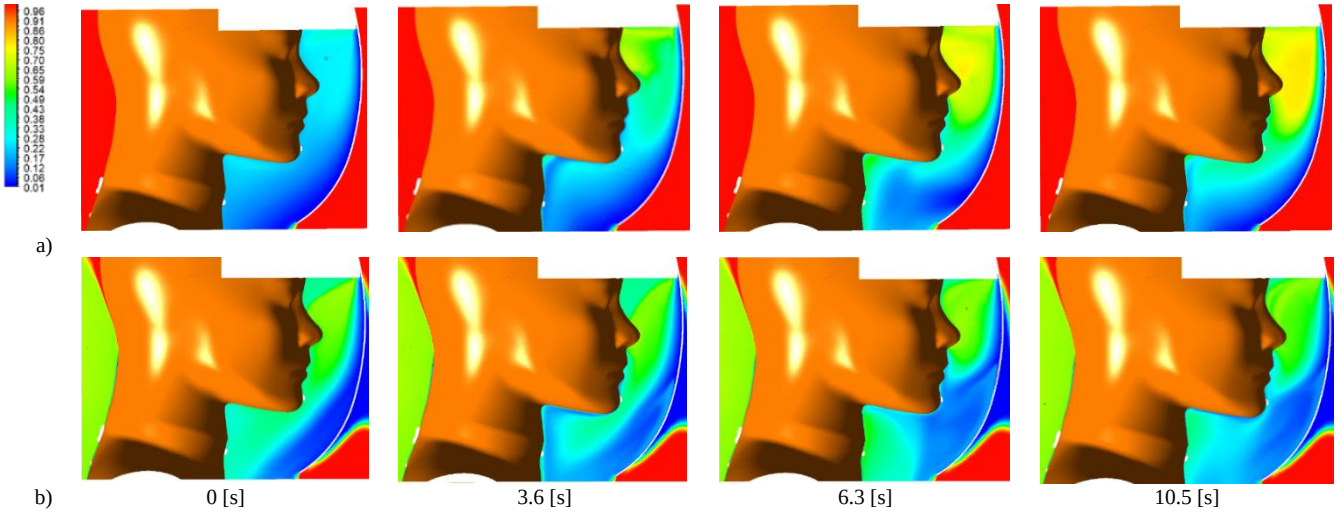

Fig. 6: Volume fraction of contaminant air in the midplane for a) RNG and b) SST turbulence models.

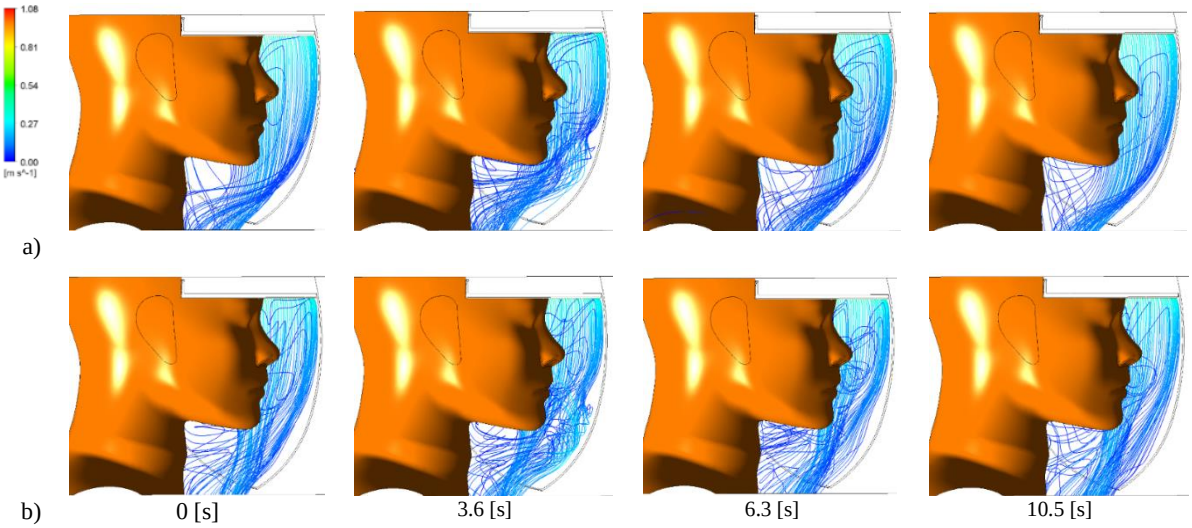

Fig. 7: Evolution of the flow streamlines for a) RNG and b) SST turbulence models.

Two optimized configurations were tested, considering the effect of breathing: one with the first velocity set and θ_4 = 20°, and the other with the fourth velocity set and θ_4 = 0°. These configurations were selected due to their higher performance out of all the optimization simulations. The BSL and SST model's results were similar. The PFs with the breathing process implemented, and without it, obtained for the first and second optimized version, for each turbulence model, are presented in Table 3. For the first optimized version, the RNG model's performance was improved by the breathing process, while the performance of the other models remained almost unchanged. The decrease in PF for the

SST and BSL models can be considered as negligible. In this configuration, the airflow from the lateral jet remained undisturbed, resulting in highly efficient visor sealing. For the RNG model, this, combined with increased recirculation inside inside the breathing zone due to the breathing effect, contributed to an improved performance. It is worth noting that the airflow mass flux for this configuration was approximately 27% higher than that of the original prototype, resulting in increased noise and energy consumption. For the second optimized version, the introduction of respiration led to a decrease decrease in the PF in all models, especially in the SST and BSL models. This was because the air curtain of this configuration configuration had lower momentum when compared with the last one, making it more "fragile". It is also worth mentioning that in this case there were fewer vortices near the mannequin's eyes, which increased the user's comfort. The mass flux of air in this configuration was half of the original mass flux, leading to less energy consumption and less noise.

Table 3: PFs of the optimized prototype with breathing and without breathing.

		RNG Model	SST Model	BSL Model
S1, $\theta_4 = 20^o$	PF with breathing	84.0 %	90.6 %	90.8 %
	PF without breathing	81.5 %	91.2 %	91.5 %
S4, $\theta_4 = 0^o$	PF with breathing	91.1 %	75.6 %	75.4 %
	PF without breathing	92.4 %	79.3 %	79.3 %

4. Conclusion

In this study, a novel PPE prototype was optimized to enhance its protection efficiency and address air suction issues from the lateral jet. The performance of the original and optimized prototypes with user respiration implemented was assessed using three turbulence models for comparison. Initially, simulations with different velocities led to an understanding of their impact on PF and the resolution of the suction problem. Lower jet velocities led to higher PF and eliminated suction from the lateral jet, with BSL and SST models generally outperforming the RNG model. Next, various tilt angles of the lateral jet were tested for two velocity sets. Optimal PF was achieved at specific angles, with significant performance drops observed for other angles. The influence of user respiration was examined, revealing differing impacts across turbulence models. Expiration improved the cleaning of the breathing zone, while inspiration facilitated polluted air entry. Among the optimized configurations, the second configuration selected for the test of the breathing simulation performed the best, offering higher PF and a stable air curtain with reduced mass flux, energy consumption, and noise compared to the original prototype. Comparing turbulence models, the RNG model consistently yielded distinct PF values, showcasing a more stable and uniform air curtain with delayed flow separation from the visor shield. Future optimizations include exploring variations in the lateral jet's outlet width and developing an optimal plenum configuration. Experimental validation of the numerical simulations is imperative for further insights.

Acknowledgments

This work was funded by FEDER - European Regional Development Funds through the operational program Centro 2020 of Portugal 2020 according to Support System for Scientific and Technological Research (SAICT) in the framework of the project "VV4MC – A new type of ventilated visor for medical care" (CENTRO-01-0145-FEDER-181248) and was sponsored by national funds through FCT – Fundação para a Ciência e a Tecnologia, under project LA/P/0079/2020, DOI: 10.54499/LA/P/0079/2020 (https://doi.org/10.54499/LA/P/0079/2020).

References

[1] M. Gholami, I. Fawad, S. Shadan, R. Rowaiee, H.A. Ghanem, A. Hassan Khamis, S.B. Ho, "COVID-19 and healthcare workers: A systematic review and meta-analysis," Int. J. Infect. Dis., vol. 104, pp. 335–346, 2021.

[2] S. Nahidi, C. Li, C. Sotomayor-Castillo, K. Kaufman-Francis, and R. Z. Shaban, "'We will have to learn to live with it': Australian dentists' experiences during the COVID-19 pandemic," Infect. Dis. Heal., vol. 27, no. 2, pp. 96–104, 2022.

[3] M. Banakar, K. Bagheri Lankarani, D. Jafarpour, S. Moayedi, M. H. Banakar, and A. MohammadSadeghi, "COVID-19 transmission risk and protective protocols in dentistry: a systematic review," BMC Oral Health, vol. 20, no. 1, p. 275, Dec. 2020.
[4] A. Ather, B. Patel, N. B. Ruparel, A. Diogenes, and K. M. Hargreaves, "Coronavirus Disease 19 (COVID-19): Implications for Clinical Dental Care," J. Endod., vol. 46, no. 5, pp. 584–595, 2020.
[5] N. Gugnani and S. Gugnani, "Safety protocols for dental practices in the COVID-19 era," Evid. Based. Dent., vol. 21, no. 2, pp. 56–57, 2020.
[6] R. J. Roberge, "Face shields for infection control: A review," J. Occup. Environ. Hyg., vol. 13, no. 4, pp. 239–246, 2016.
[7] L. Meng, F. Hua, and Z. Bian, "Coronavirus Disease 2019 (COVID-19): Emerging and Future Challenges for Dental and Oral Medicine," J. Dent. Res., vol. 99, no. 5, pp. 481–487, 2020.
[8] J. Hamilton, T. Lewis, L. Farmer, and D. Richards, "Universal visors as a key measure to stop nosocomial transmission of SARS-CoV-2," J. Hosp. Infect., vol. 111, pp. 200–201, 2021.
[9] X. Zhang, H. Li, S. Shen, and M. Cai, "Investigation of the flow-field in the upper respiratory system when wearing N95 filtering facepiece respirator," J. Occup. Environ. Hyg., vol. 13, no. 5, pp. 372–382, 2016.
[10] M. Goto, N. Ueckert, R. K. Meiches, and E. N. Perencevich, "Successful multimodal measures preventing coronavirus disease 2019 (COVID-19) outbreaks without universal frequent testing within long-term care units in the Midwestern Veterans' Health Care Network," Infect. Control Hosp. Epidemiol., vol. 42, no. 12, pp. 1503–1505, 2021.
[11] M. J. Woodfield, R. M. Jones, and D. K. Sleeth, "Influence of face shields on exposures to respirable aerosol," J. Occup. Environ. Hyg., vol. 19, no. 3, pp. 139–144, 2022.
[12] A. S. Sakharov and K. Zhukov, "Study of an Air Curtain in the Context of Individual Protection from Exposure to Coronavirus (SARS-CoV-2) Contained in Cough-Generated Fluid Particles," Physics (College. Park. Md)., vol. 2, no. 3, pp. 340–351, 2020.
[13] M. S. Alshitawi, S. Suyambazhahan, and A. S. Alaboodi, "Computational fluid dynamics simulation of breathing zone of the human for air quality with a personalized air curtain," Adv. Mech. Eng., vol. 11, no. 5, pp. 1–13, 2019.
[14] X. Wei, D. Yi, W. Xie, J. Gao, and L. Lv, "Protection against inhalation of gaseous contaminants in industrial environments by a personalized air curtain," Build. Environ., vol. 206, no. August, p. 108343, 2021.
[15] J. Ma, H. Qian, F. Liu, and X. Zheng, "Performance analysis of a novel personalized air curtain for preventing inhalation of particulate matters in industrial environments," J. Build. Eng., vol. 58, no. July, p. 105014, 2022.
[16] N. Rosa, M. Jordão, J. Costa, A. Gaspar, N. Martinho, A. Gameiro Lopes, M. Panão, M. Gameiro da Silva, "Experimental and numerical evaluation of a new visor concept with aerodynamic sealing to protect medical professionals from contaminated droplets and aerosols," Indoor Air, vol. 32, no. 9, pp. 1–14, 2022.
[17] N. Rosa, A. R. Gaspar, J. J. Costa, A. G. Lopes, J. Sabino Pais, and M. Gameiro da Silva, "Experimental assessment of an air curtain-sealed personal protective equipment for medical care: influence of breathing and thermal plume," Exp. Therm. Fluid Sci., p. 110955, May 2023.
[18] J. Mota, N. Rosa, A. R. Gaspar, J. J. Costa, A. G. Lopes, and M. Gameiro da Silva, "Acoustic assessment of a novel visor concept with aerodynamic sealing for medical care," Appl. Acoust., vol. 217, no. September 2023, p. 109852, 2024.
[19] J. Pan, C. Harb, W. Leng, and L. C. Marr, "Inward and outward effectiveness of cloth masks, a surgical mask, and a face shield," Aerosol Sci. Technol., vol. 55, no. 6, pp. 718–733, 2021.
[20] N. Gao and J. Niu, "Transient CFD simulation of the respiration process and inter-person exposure assessment," Build. Environ., vol. 41, no. 9, pp. 1214–1222, 2006.